







# Low-Loss Fluoride Optical Fiber Coupler for Mid-Infrared Applications

Francesco Anelli , *Student Member, IEEE*, Andrea Annunziato , Antonella Maria Loconsole ,  
Vincenza Portosi , Solenn Cozic , Paul Le Pays du Teilleul, Sebastien Venck, Samuel Poulain,  
and Francesco Prudeniano , *Member, IEEE*

**Abstract**—For the first time, a  $2 \times 2$  optical fiber coupler based on indium fluoride optical fibers is designed via coupled mode theory, fabricated via fused biconical tapering technique, and characterized in the mid-infrared spectral range. A conventional glass processing system, Vytran GPX-2400, is employed for the  $2 \times 2$  optical fiber coupler fabrication, overcoming the main limitation related to the narrow temperature range for indium fluoride optical fiber processing. Moreover, the fabricated device exhibits negligible surface crystallizations. The experimental results are in optimum agreement with the simulations, demonstrating that reproducible manufacturing of low-loss fused optical fiber components for the mid-infrared spectral range is possible. In particular, the fabricated  $2 \times 2$  optical fiber coupler is characterized by a measured coupling ratio  $C_R = 72.2:27.8$  at the wavelength  $\lambda = 3.34 \mu\text{m}$ , with low excess loss  $E_L = 0.88 \text{ dB}$ .

**Index Terms**—Coupled mode theory, fused optical fiber components, modeling, optical couplers, soft glasses.

## I. INTRODUCTION

MID-INFRARED (Mid-IR) wavelength advances are drawing research attention, since they are opening novel perspectives in many fields, including sensing, spectroscopy, imaging, light sources, and comb generation [1], [2], [3], [4],

Manuscript received 7 August 2023; revised 9 November 2023; accepted 27 November 2023. Date of publication 29 November 2023; date of current version 2 April 2024. This work was supported in part by the European Union under the Italian National Recovery and Resilience Plan (NRRP) of NextGenerationEU, “Telecommunications of the Future” (PE00000001 - Program “RESTART”, CUP: D93C22000910001) - DREAMS - Antennas and Devices for mixing, Detection, and Manipulation of mmWaves, in part by MIUR “Agriculture Green & Digital – AGREED”, PNR 2015/20, n. ARS01\_00254; H2020-ICT-37-2020 “Photonic Accurate and Portable Sensor Systems Exploiting Photo-Acoustic and Photo-Thermal Based Spectroscopy for Real-Time Outdoor Air Pollution Monitoring – PASSEPARTOUT” n. 101016956, and in part by MIUR PRIN 2022, NRPP – DD n. 1181 del 27-07-2023 - Innovative Technologies for non-invasive assessment of plant health condition to support precision farming (VEGETATION). (Corresponding author: Francesco Prudeniano.)

This work did not involve human subjects or animals in its research.

Francesco Anelli, Andrea Annunziato, Antonella Maria Loconsole, Vincenza Portosi, and Francesco Prudeniano are with the Department of Electrical and Information Engineering, Politecnico di Bari, 70126 Bari, Italy (e-mail: francesco.anelli@poliba.it; andrea.annunziato@poliba.it; antonellamaria.loconsole@poliba.it; vincenza.portosi@poliba.it; francesco.prudeniano@poliba.it).

Solenn Cozic, Paul Le Pays du Teilleul, Sebastien Venck, and Samuel Poulain are with the Le Verre Fluoré, 35170 Bruz, France (e-mail: solenn.cozic@leverrefluore.com; paul.duteilleul@leverrefluore.com; sebastien.venck@leverrefluore.com; samuel.poulain@leverrefluore.com).

Color versions of one or more figures in this article are available at <https://doi.org/10.1109/JLT.2023.3337603>.

Digital Object Identifier 10.1109/JLT.2023.3337603

[5], [6]. Anyway, the Mid-IR technology maturity is still inadequate, because the essential building blocks required in laser and amplifier systems such as couplers, combiners, and splitters, operating in this spectral range, are not yet sufficiently developed [7].

Mid-IR optical fibers are generally manufactured with chalcogenide glasses (containing sulfur, selenium, and/or tellurium) and fluoride glasses (zirconium fluoride glass, and indium fluoride glass) [8]. Chalcogenide optical fibers have been widely investigated because of their large band of low-attenuation, the high nonlinear coefficient, and the possibility to obtain active optical fibers through rare-earths doping [8]. These strength points are common with fluoride optical fibers, which offer extremely low Rayleigh scattering and low attenuation with the possibility to guide light in the transmission window  $\lambda = 0.3 \div 4.5 \mu\text{m}$  for zirconium fluoride glass and in the range  $\lambda = 0.3 \div 5.5 \mu\text{m}$  for indium fluoride glass [9], [10]. Moreover, fluoride fibers show low Fresnel losses at the interface with air or silica [11], [12]. One of the key building blocks of most optical fiber systems is the optical fiber coupler, essential for multiplexing/demultiplexing, signal/pump combination, ring cavities, filters, etc. [13], [14].

The first experiments performed on soft glasses optical fiber couplers date to early 90s [15], [16]. Most of the successive studies concerned broadband, wavelength-dependent and nonlinear chalcogenide couplers with different coupling ratios  $C_R$  [7], [17], [18], [19], [20], [21], [22]. Side-polished bonding and fused biconical tapering techniques have been exploited for the construction of zirconium fluoride couplers [11], [15], [23], [24], [25], [26], [27]. The fused biconical tapering technique is considered better than side-etching and side-polishing with reference to reliability and repeatability [18]. When dealing with fluoride optical fibers, the glass fragility, and the steep viscosity/temperature characteristic should be taken into account [10]. The latter implies the need for precise temperature control to avoid surface crystallization, which may lead to high excess loss  $E_L$ . Indeed, the couplers fabricated with fluoride optical fibers suffer from relatively high excess losses  $E_L$  [24], [25], [26], [27]. Therefore, some technological issues need to be further explored to address the requirement for low-loss devices operating in the mid-infrared [28].

In this paper, for the first time to the best of our knowledge, we propose the design, the fabrication and the characterization, in the mid-infrared spectral range, of a low-loss  $2 \times 2$  optical coupler based on indium fluoride ( $\text{InF}_3$ ) optical fibers from Le

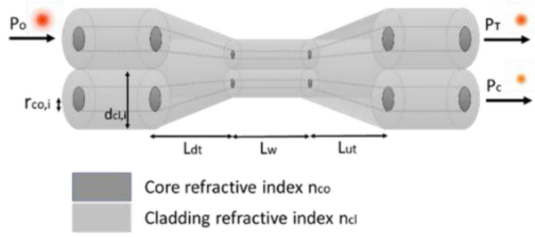


Fig. 1. Sketch of an optical fiber coupler fabricated via fused biconical tapering technique; the input power  $P_0$  is split among the through port and the cross port, according to the physical and geometrical properties of the waist/coupling region, long  $L_w$ .

Verre Fluoré (Bruz, France). The  $2 \times 2$  optical coupler is fabricated via Vytran GPX-2400 glass processing system adopting a single-sweep technique. The total tapering time is  $\sim 100$  s, faster than multi-sweep technique [29]. Two step-index optical fibers are stacked inside a low refractive index indium fluoride capillary and tapered down to  $\sim 23\%$  of their initial diameter. The through port and the cross port powers of the coupler are characterized at the wavelength  $\lambda = 3.34 \mu\text{m}$ , employing a pigtailed Interband Cascade Laser (ICL).

The paper is organized as follows. Section II reports an overview of the optical fiber coupler operating principle; Section III, the electromagnetic design of the optical fiber coupler; Section IV, the fabrication process via commercial glass processing system; Section V, the characterization of the device in the mid-infrared spectral range; Section VI, the conclusion and the prospects.

## II. OPTICAL FIBER COUPLER OPERATING PRINCIPLE

$2 \times 2$  optical fiber couplers are typically employed to split or combine the light with low excess loss  $E_L$ , at the desired coupling ratio  $C_R$  [17]. Optical fiber couplers can be fabricated via fused biconical tapering technique, in which two optical fibers, placed in close contact with each other, are heated and stretched over a short distance. The power coupling between the electromagnetic modes occurs in the waist region, i.e., the region with the smallest diameter, see Fig. 1, where the well-known periodic exchange of power between the electromagnetic modes is experienced. Coupled mode theory is usually employed in the electromagnetic design to describe the codirectional coupling for  $HE_{11}$  mode [7], [17]. In a symmetric coupler, the input power  $P_0$  is injected in the input port and then split between the cross port  $P_C$  and the through port  $P_T$ , according to [7], [17]:

$$P_C = P_0 \sin^2(\kappa L_w) \quad (1)$$

$$P_T = 1 - P_C = P_0 \cos^2(\kappa L_w) \quad (2)$$

$$U = r_{co,f} \sqrt{n_{co}^2 k_0^2 - \beta^2} \quad (3)$$

$$W = r_{co,f} \sqrt{\beta^2 - n_{cl}^2 k_0^2} \quad (4)$$

$$\kappa = \frac{K_0 \left( \frac{WD}{r_{co,f}} \right) U^2}{k_0 n_{co} (r_{co,f} V K_1(W))^2} \quad (5)$$

where the equation parameters are the following:  $\kappa$  the coupling coefficient,  $L_w$  the waist length,  $K_0$ , and  $K_1$  the zeroth and first order Bessel functions of the second kind (respectively evaluated at  $\frac{WD}{r_{co,f}}$  and  $W$ ),  $r_{co,f}$  the core radius in the waist region,  $D$  the core-to-core distance in the waist region,  $n_{co}$  the core refractive index,  $n_{cl}$  the cladding refractive index,  $k_0$  the free-space wave number,  $\beta$  the propagation constant,  $V$  the normalized frequency.

The performance of a  $2 \times 2$  optical fiber coupler is described by the excess loss  $E_L$  and coupling ratio  $C_R$  [30].

$$E_L = 10 \log_{10} (P_0 / (P_T + P_C)) \quad (6)$$

The coupling ratio  $C_R$  is related to the optical power of each output port divided by the sum of the powers at the two output ports [30]:

$$C_{R-T} = P_T / (P_T + P_C) \quad (7)$$

$$C_{R-C} = P_C / (P_T + P_C) \quad (8)$$

The coupling ratio  $C_R$  and its spectral dependence are strictly dependent on the geometry of the optical fiber coupler. The excess loss  $E_L$  is affected by the quality and the geometry of the transition. To avoid higher order cladding modes coupling, the transition must be adiabatic [31].

The taper transition is adiabatic when the core radius  $r_{co}$  of the optical fiber slowly decreases along the taper length  $L_{dt}$ . In a multimode optical fiber, the radius of the core  $r_{co}(z)$ , expressed as a function of the propagation direction  $z$ , must change by satisfying the following condition:

$$\frac{dr_{co}}{dz} \leq \frac{r_{co}(z)}{Z_p} \quad (9)$$

where  $Z_p = 2r_{co}/\tan(\alpha)$  is the half period between reflections,  $NA = \sin(\alpha)$  is the optical fiber numerical aperture, and  $\alpha$  is the ray angle [32], [33]. The minimum taper transition length  $L_{dt,\min}$  can be calculated from (9), according to:

$$L_{dt,\min} \geq \frac{2(r_{co,i} - r_{co,f})}{\tan(\alpha)} \quad (10)$$

where  $r_{co,i}$  and  $r_{co,f}$  are the fiber core radii before and after the tapering, respectively.

## III. OPTICAL FIBER COUPLER DESIGN

The  $2 \times 2$  indium fluoride optical fiber coupler electromagnetic design is carried out via coupled mode theory to estimate the through and the cross port powers for different waist geometries [34], [35]. The designed optical fiber coupler is made of two step-index indium fluoride fibers IFG MM (0.20) 28/100 from Le Verre Fluoré (Bruz, France), having core diameter  $d_{co,i} = 28 \mu\text{m}$  and cladding diameter  $d_{cl,i} = 100 \mu\text{m}$ . The cladding diameter is smaller than that of the typical optical fibers (i.e.,  $d_{cl,i} = 125 \mu\text{m}$ ) to assist the mode coupling in the waist region. The optical fibers are inserted within a capillary with low refractive index. The capillary allows the close contact of the optical fibers, makes the optical fiber coupler robust, and facilitates the fusion process, since the larger cross-sectional area allows for making the control of the fabrication parameters less

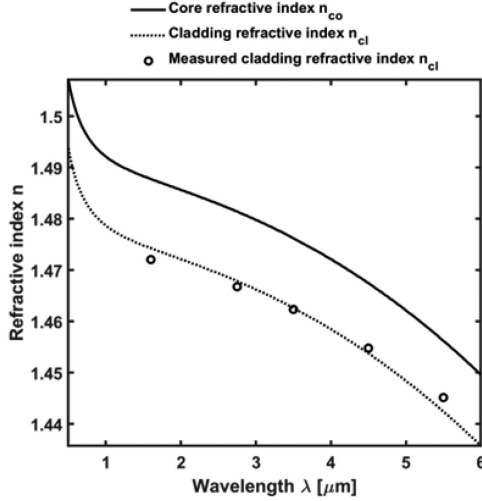


Fig. 2. Dispersion of the core refractive index  $n_{co}$  (solid line) and of the cladding refractive index  $n_{cl}$  (dotted line) as functions of the wavelength  $\lambda$ .

demanding. The capillary inner diameter is  $d_{in-cap,i} = 360 \mu\text{m}$ , the capillary output diameter is  $d_{out-cap,i} = 550 \mu\text{m}$ .

The core and cladding refractive indices, at the wavelength  $\lambda = 3.34 \mu\text{m}$ , are respectively  $n_{co} = 1.4774$  and  $n_{cl} = 1.4638$ , resulting in a numerical aperture  $NA \sim 0.20$ . The capillary refractive index is  $n_{cap} = 1.4618$  at the same wavelength  $\lambda = 3.34 \mu\text{m}$ . Fig. 2 reports the refractive index dispersion of the core refractive index  $n_{co}$  (solid line) and of the cladding refractive index  $n_{cl}$  (dotted line) as functions of the wavelength  $\lambda$ , used for simulations. In particular, the dispersion equations reported in [36] have been employed with slightly changed weights to better fit the measured values of the cladding refractive index, obtained via Littrow method at room temperature (circle markers) [37]. The effect of potential glass component interdiffusion is neglected, so that the waist region is just a scaled-down version of the non-tapered geometry.

The effective refractive index of the mode guided in the waist region of each optical fiber, in the absence of the other optical fiber, is  $n_{eff} \sim 1.4647$  at the wavelength  $\lambda = 3.34 \mu\text{m}$ , calculated via finite element method (FEM) simulation. The electric field norm of the supermode guided in the waist region (i.e., related to the linear combination of the  $HE_{11}$  mode guided in each optical fiber), having practically the same effective refractive index  $n_{eff} \sim 1.4647$ , is reported in Fig. 3 and shows the field overlapping. The desired coupling ratio  $C_R = 70:30$  is obtained with a waist length  $L_W = 21.25 \text{ mm}$  and a scaling factor  $SF = 4.3$ . Therefore, the designed core radius in the waist region is  $r_{co,f} = r_{co,i} / SF = 14 \mu\text{m} / 4.3 = 3.26 \mu\text{m}$  and the core-to-core distance in the waist region is  $D = d_{cl,i} / SF = 100 \mu\text{m} / 4.3 = 23.26 \mu\text{m}$ . The optical fibers are single mode in the waist region. Down-taper and up-taper have the same length  $L_{dt} = L_{ut} = 15 \text{ mm}$ ; adiabatic transitions are designed to avoid losses related to higher order modes coupling [34].

Fig. 4 reports the spectral dependance of the normalized output powers of the through port  $P_T$  (solid line) and of the cross port  $P_C$  (dotted line).

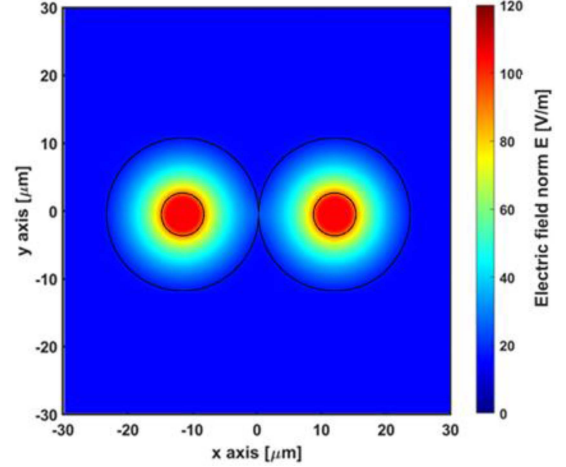


Fig. 3. Electric field norm  $E$  of the supermode guided in the waist region; scaling factor  $SF = 4.3$ , supermode effective refractive index  $n_{eff} \sim 1.4647$ , at the wavelength  $\lambda = 3.34 \mu\text{m}$ .

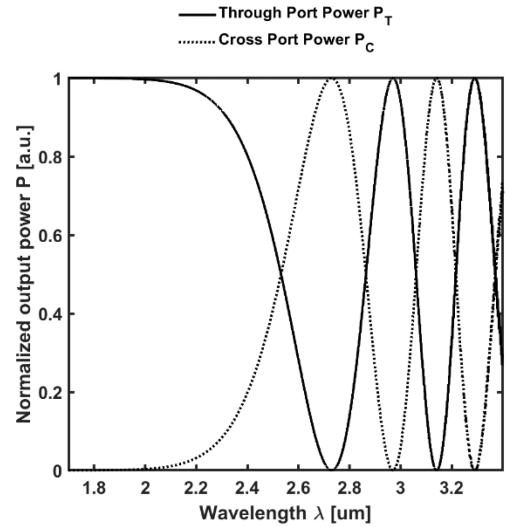


Fig. 4. Normalized output powers of the through port  $P_T$  (solid line) and of the cross port  $P_C$  (dotted line) as functions of the wavelength  $\lambda$ .

Fig. 5 reports the normalized output powers of the through port  $P_T$  (solid line) and of the cross port  $P_C$  (dotted line), as functions of the waist length  $L_w$ , at the wavelength  $\lambda = 3.34 \mu\text{m}$ .

The design is also validated via 3D-Beam Propagation Method (BPM, BeamProp, RSoft Design Group). The input optical fiber is excited with a Gaussian beam with beam waist  $B_W = 31 \mu\text{m}$ . Coincident coupling ratio  $C_R$  is obtained.

#### IV. OPTICAL FIBER COUPLER FABRICATION

Two segments of IFG MM (0.20) 28/100 are cleaved through Vytran LDC-400 optical fiber cleaver. The cross-sections are inspected with the microscope, to prevent the presence of scratches on the optical fiber end-facets. The optical fiber segments are inserted in the low-index capillary, with the help of isopropyl alcohol. Alcohol excesses are then removed by the vacuum pump Linicon LV-125A. The length of the low-index capillary

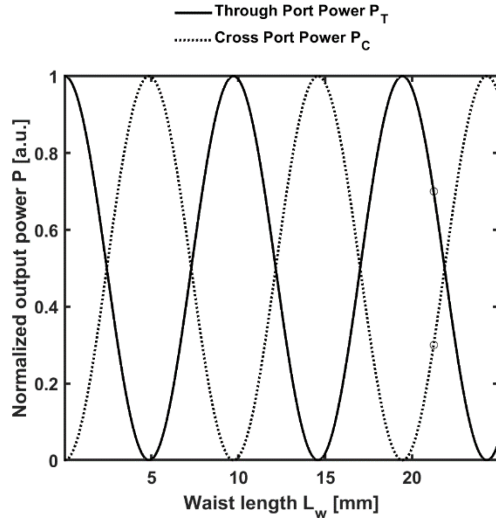


Fig. 5. Normalized output powers of the through port  $P_T$  (solid line) and of the cross port  $P_C$  (dotted line) as functions of the waist length  $L_w$ , at the wavelength  $\lambda = 3.34 \mu\text{m}$ .

TABLE I  
MAIN PARAMETERS FOR VYTRAN GPX-2400 PROCESSING SYSTEM [38]

Parameter	Value	Description
$P$	12.1 W	Initial filament power
$v_{FHB}$	500 $\mu\text{m/s}$	Fiber holding block pull velocity
$T_0$	19 g	Initial tension
$F_{Ar}$	0.35 L/min	Argon flow rate during the process

is  $L_{cap} = 17$  cm. The optical fibers are not twisted to avoid potential bend loss. The structure is clamped in the fiber holding blocks of the Vytran GPX-2400 glass filament processing system. The room temperature is  $T_r \sim 20^\circ\text{C}$ , the room humidity is  $RH \sim 30\%$ . The drawbacks of indium fluoride glass include the mechanical fragility, the physical behavior dependent on temperature and room humidity level, the surface oxidation, the glass viscosity, and the interdiffusion of core/cladding/capillary materials [10]. Some of these downsides can be mitigated by making sure that the graphite filament operates near the glass transition temperature  $T_g \sim 275^\circ\text{C}$  for the entire fabrication process and the heating is performed under controlled environment (i.e., argon flow) [38]. The main parameters pertaining the fabrication via Vytran GPX-2400 glass filament processing system are identified through trial-and-error technique and reported in Table I.

For the correct identification of the fabrication parameters, the optical fiber coupler transition quality, the matching between the imposed and the measured dimensions, and the drawing tension characteristic during the fabrication process are considered. For a fixed value of the fiber holding block pull velocity  $v_{FHB}$ , a high filament power  $P$  may lead to surface crystallization, small waist diameter, or impossibility of completing the fused biconical taper. Otherwise, a low filament power may lead to big waist diameter, or capillary/optical fibers breaking. Fig. 6 shows the drawing tension  $T$  during the fabrication time  $t$ , useful to

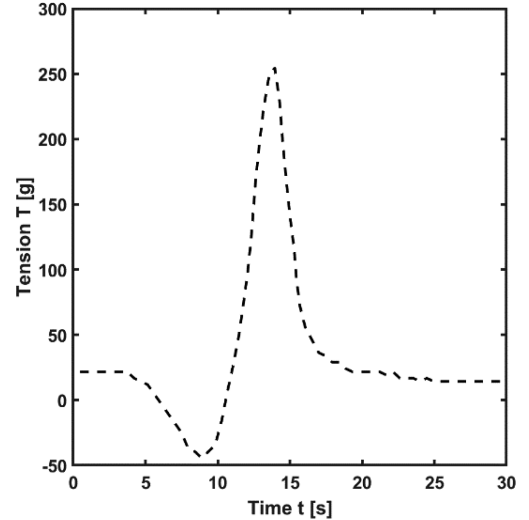


Fig. 6. Drawing tension  $T$  as a function of the fabrication time  $t$ .

identify the correct value for the initial filament power  $P$ , for the fiber holding block pull velocity  $v_{FHB}$  reported in Table I.

In particular, if the peak is negative, or close to  $0\text{g}$ , the glass is over softened or melted, leading to visible surface crystallization.

On the contrary, if the peak is too high, the initial filament power  $P$  must be increased since the glass has not reached the softening temperature  $T_g$ .

The measured waist length is  $L_W \sim 21$  mm, the capillary cross-section in the waist region is elliptical, characterized by semi-axes  $a \sim 70 \mu\text{m}$  and  $b \sim 90 \mu\text{m}$ . The length of the semi-axis  $b$ , which is the most significant, is in good agreement with the imposed scaling factor  $SF = 4.3$ , i.e.,  $b = (2 \times d_{cl,i} + d_{out-cap,i} - d_{in-cap,i})/SF = 90.70 \mu\text{m}$ . In Fig. 7, a montage of the longitudinal micrographs captured by Vytran GPX-2400 CCD camera is reported.

A smooth reduction in diameter is achieved without any irregularity in the taper profile. Despite the presence of some surface crystallization, it is possible to achieve low excess loss  $E_L$ . To ensure minimal losses, it is crucial to avoid crystallization in the areas where the electromagnetic field is guided.

## V. OPTICAL FIBER COUPLER CHARACTERIZATION

The schematic of the experimental set-up is reported in Fig. 8. The fabricated device is tested via an ICL, Nanoplus Nanosystems and Technologies GmbH (Wurzburg, Germany), emitting at  $\lambda = 3.34 \mu\text{m}$ . The ICL has been pigtailed with indium fluoride optical fiber IFG (0.30) 9.5/125, Le Verre Fluoré (Bruz, France). The electromagnetic mode field diameter of the IFG (0.30) 9.5/125 optical fiber is  $MFD = 9.7 \mu\text{m}$ .

The excitation is performed with free-space coupling, by means of a groove and Thorlabs MAX313D/M 3-axis stage.

The through  $P_T = 2.59$  mW and cross  $P_C = 1.00$  mW port powers are read by two thermal power sensors, i.e., PW 1 and PW 2, connected to Thorlabs PM100D console, see Fig. 8.

The fabricated coupler waist length is slightly shorter than the designed one. As a consequence, the measured coupling



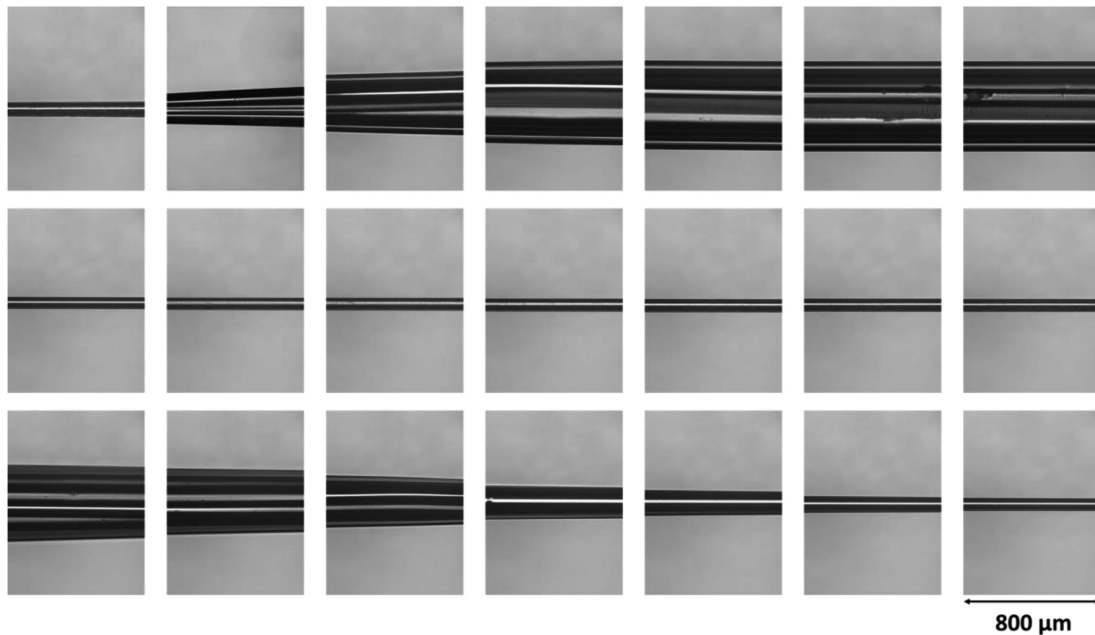


Fig. 7. Montage of longitudinal micrographs (starting from top right, finishing to bottom left) of the fabricated  $2 \times 2$  indium fluoride optical fiber coupler, captured via CCD camera. Each micrograph covers a length of  $800 \mu\text{m}$ . Micrographs are reported with a sampling step of  $1600 \mu\text{m}$ .

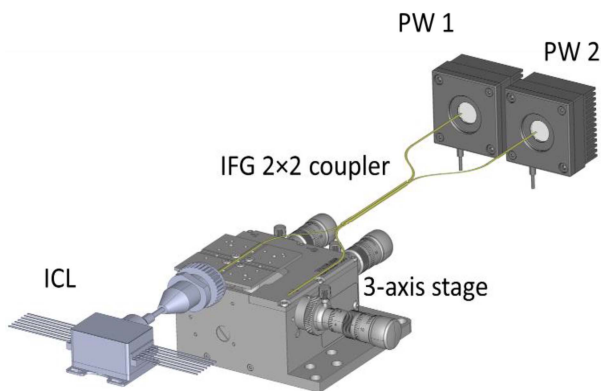


Fig. 8. Sketch of the experimental set-up adopted to characterize the fabricated  $2 \times 2$  indium fluoride optical fiber coupler. The ICL power is coupled in the input optical fiber of the coupler via Thorlabs MAX313D/M 3-axis stage. The cross port power  $P_C$  and the through port power  $P_T$  are measured with two thermal power sensors, i.e., PW 1 and PW 2.

ratio is  $C_R = 72.2 : 27.8$ , very close but not coincident with the nominal value  $C_R = 70 : 30$ . The power injected in the input optical fiber of the coupler is  $P_0 = 4.4 \text{ mW}$ . This value has been measured after having cleaved the input optical fiber immediately before the down-taper region, without varying the input coupling condition. The excess loss is  $E_L = 0.88 \text{ dB}$  and takes into account also the losses induced from the reduction of the modes number in the down-taper transition [39]. Indeed, the starting geometry is a few-mode optical fiber and only the fundamental mode is guided in the waist/coupling region.

Better excess loss  $E_L$  could be obtained by exploiting single-mode optical fibers. However, the achieved performance is remarkably high also with reference to the state of the art, as it can be inferred by Table II.

TABLE II  
PERFORMANCE COMPARISON BETWEEN FLUORIDE OPTICAL FIBER COUPLERS

Ref.	Glass	Operation	Wavelength $\lambda$	Coupling Ratio $C_R$	Excess Loss $E_L$
[24]	Zirconium fluoride	Multimode	$2.00 \mu\text{m}$	50:50	3.0 dB
[25]	Zirconium fluoride	Single-mode	$2.20 \mu\text{m}$	14:86	1.8 dB
[26]	Zirconium fluoride	Single-mode	$2.70 \mu\text{m}$	61:39	4.3 dB
[27]	Zirconium fluoride	Single-mode	$2.73 \mu\text{m}$	41:59	2.5 dB
This work	Indium fluoride	Few-mode	$3.34 \mu\text{m}$	72.2:27.8	0.88 dB

To assess the effects of aging on losses, the device is tested after one month. Negligible variations, within the set-up measurement uncertainty, have been observed in terms of excess loss  $E_L$  and coupling ratio  $C_R$ .

The optical fiber coupler can be adapted for operation at longer wavelengths, up to  $\lambda = 5.5 \mu\text{m}$ , which is upper transparency limit of the  $\text{InF}_3$  glass. To operate at longer wavelengths, smaller scaling factor SF is required. As an example, the scaling factor  $SF = 2.6$  and the waist length  $L_W = 8.2 \text{ mm}$  are suitable for an optical fiber coupler with the same coupling ratio  $C_R = 70 : 30$  operating at the wavelength  $\lambda = 5.0 \mu\text{m}$ . This last coupler is easier to be fabricated and mechanically more robust.

## VI. CONCLUSION

For the first time, a low-loss optical fiber coupler based on indium fluoride optical fibers has been designed, fabricated, and characterized in the mid-infrared spectral range. The measured coupling ratio is  $C_R = 72.2 : 27.8$ , while the excess loss is

$E_L = 0.88$  dB at the wavelength  $\lambda = 3.34 \mu\text{m}$ . The experimental results are in optimum agreement with the simulation. Further research efforts will be focused on exploring the power-damage threshold of the indium fluoride optical fiber coupler. The fabricated coupler encourages and boosts the research towards all-in-fiber mid-infrared applications, e.g., in-band pumped mid-infrared amplifiers and high-power all-in-fiber lasers.

#### ACKNOWLEDGMENT

The authors would like to thank Nanoplus Nanosystems and Technologies GmbH (Wurzburg, Germany) and Dr. Robert Weih for the ICL source optimization.

#### REFERENCES

- [1] R. Bartlome and M. W. Sigrist, "Laser-based human breath analysis: D/H isotope ratio increase following heavy water intake," *Opt. Lett.*, vol. 34, no. 7, pp. 866–868, 2009.
- [2] S. Dupont, C. Petersen, J. Thøgersen, C. Agger, O. Bang, and S. R. Keiding, "IR microscopy utilizing intense supercontinuum light source," *Opt. Exp.*, vol. 20, no. 5, pp. 4887–4892, 2012.
- [3] B. Kuyken et al., "An octave-spanning mid-infrared frequency comb generated in a siliconnanophotonic wire waveguide," *Nature Commun.*, vol. 6, 2015, Art. no. 6310.
- [4] A. M. Loconsole, M. C. Falconi, V. Portosi, and F. Prudenzano, "Numerical design of a gain-switched pulsed laser at  $3.92 \mu\text{m}$  wavelength based on a Ho<sup>3+</sup>-doped fluoroindate fiber," *J. Lightw. Technol.*, vol. 39, no. 10, pp. 3276–3283, May 2021.
- [5] G. Scurria, I. Manek-Hönninger, S. Bigotta, A. Dholand, and J. I. Carrée, "7 W mid-infrared supercontinuum generation up to  $4.7 \mu\text{m}$  in an indium fluoride optical fiber pumped by a high-peak power thulium-doped fiber single-oscillator," *Opt. Exp.*, vol. 28, pp. 7672–7677, 2020.
- [6] A. M. Loconsole, M. C. Falconi, A. Annunziato, S. Cozic, S. Poulain, and F. Prudenzano, "Design of a mid-IR laser based on a Ho:Nd-codoped fluoroindate fiber," *J. Lightw. Technol.*, vol. 41, no. 2, pp. 702–708, Jan. 2023.
- [7] F. Tavakoli, A. Rezik, and M. Rochette, "Broadband and wavelength-dependent chalcogenide optical fiber couplers," *IEEE Photon. Technol. Lett.*, vol. 29, no. 9, pp. 735–738, May 2017.
- [8] D. Cai, Y. Xie, X. Guo, P. Wang, and L. Tong, "Chalcogenide glass microfibers for mid-infrared optics," *Photonics*, vol. 8, no. 11, 2021, Art. no. 497.
- [9] M. Saad, "Fluoride glass fiber: State of the art," *Proc. SPIE*, vol. 7316, 2009, Art. no. 73160N.
- [10] É. Ducharme, S. Virally, R. I. Becerra-Deana, C. Boudoux, and N. Godbout, "Viscosity of fluoride glass fibers for fused component fabrication," *Appl. Opt.*, vol. 61, pp. 5031–5039, 2022.
- [11] R. R. Gattass, R. Thapa, F. H. Kung, L. E. Busse, L. B. Shaw, and J. S. Sanghera, "Review of infrared fiber-based components," *Appl. Opt.*, vol. 54, no. 31, pp. F25–F34, 2015.
- [12] C. Florea, J. Sanghera, L. Busse, B. Shaw, F. Miklos, and I. Aggarwal, "Reduced Fresnel losses in chalcogenide fibers obtained through fiber-end microstructuring," *Appl. Opt.*, vol. 50, no. 1, pp. 17–21, 2011.
- [13] M. Rezaei and M. Rochette, "All-chalcogenide ring fiber laser," *Opt. Fiber Technol.*, vol. 71, 2022, Art. no. 102900.
- [14] Q. Xiao, X. Chen, H. Ren, P. Yan, and M. Gong, "Fiber coupler for mode selection and high-efficiency pump coupling," *Opt. Lett.*, vol. 38, pp. 1170–1172, 2013.
- [15] V. C. d. Foresto and S. Ridgway, "FLUOR: A stellar interferometer using single-mode infrared fibers," in *High-resolution Imaging By Interferometry II Eds*, J. Beckers and F. Merkle Ed. Garching, Germany: ESO, 1991, pp. 731–740.
- [16] I. Tugendhaft, A. Bornstein, Y. Weissman, and A. A. Hardy, "Directional multimode fiber couplers in the mid-infrared," *Proc. SPIE*, vol. 34, no. 10, pp. 2846–2849, 1995.
- [17] M. Rezaei and M. Rochette, "All-chalcogenide single-mode optical fiber couplers," *Opt. Lett.*, vol. 44, no. 21, pp. 5266–5269, 2019.
- [18] O. Benderov et al., "Broadband mid-IR chalcogenide fiber couplers," *Appl. Opt.*, vol. 58, no. 26, pp. 7222–7226, 2019.
- [19] B. Stepanov, O. Benderov, T. Tebeneva, G. Snopatin, M. Spiridonov, and I. Scripachev, "Chalcogenide optical fiber couplers made by FBT method," *J. Non-Cryst.*, vol. 480, pp. 23–27, 2018.
- [20] D. T. Schaafsma, J. A. Moon, J. S. Sanghera, and I. D. Aggarwal, "Fused taper infrared optical fiber couplers in chalcogenide glass," *J. Lightw. Technol.*, vol. 15, no. 12, pp. 2242–2245, Dec. 1997.
- [21] M. Rezaei, M. H. M. Shamim, M. E. Amraoui, Y. Messaddeq, and M. Rochette, "Nonlinear optical fiber couplers made of chalcogenide glass," in *Proc. Conf. Lasers Electro-Opt., Tech. Dig. Ser.*, 2022, Paper AT4C.7.
- [22] M. Rezaei, M. H. M. Shamim, M. El Amraoui, Y. Messaddeq, and M. Rochette, "Nonlinear chalcogenide optical fiber couplers," *Opt. Exp.*, vol. 30, no. 12, pp. 20288–20297, 2022.
- [23] S. T. Nicholls and M. Scott, "Method of making fluoride glass optical coupler," U.S. Patent US5139550 A, Aug. 1992.
- [24] G. Stevens and T. Woodbridge, "Mid-IR fused fiber couplers," *Proc. SPIE*, vol. 9730, 2016, Art. no. 973007.
- [25] M. Rezaei and M. Rochette, "Single-mode ZBLAN optical fiber couplers," in *Proc. Optica Adv. Photon. Congr. 2022, Tech. Dig. Ser.*, 2022, Paper ITh2B.3.
- [26] M. Rezaei, G. T. Zeweldi, M. H. M. Shamim, and M. Rochette, "Single mode optical fiber couplers made of ZBLAN glass," in *Proc. Optica Adv. Photon. Congr.*, 2023, Paper STh3G.3.
- [27] M. Rezaei, G. T. Zeweldi, M. H. M. Shamim, and M. Rochette, "Single-mode optical fiber couplers made of fluoride glass," *Opt. Exp.*, vol. 31, pp. 27183–27191, 2023.
- [28] W. C. Wang, B. Zhou, S. H. Xu, Z. M. Yang, and Q. Y. Zhang, "Recent advances in soft optical glass fiber and fiber lasers," *Prog. Mater. Sci.*, vol. 101, pp. 90–171, 2019.
- [29] C. Baker and M. Rochette, "A generalized heat-brush approach for precise control of the waist profile in fiber tapers," *Opt. Mater. Exp.*, vol. 1, pp. 1065–1076, 2011.
- [30] I. Yokohama, K. Chida, and J. Noda, "Low excess loss conditions of polarization-maintaining fiber couplers," *Appl. Opt.*, vol. 27, no. 23, pp. 4807–4813, 1988.
- [31] J. D. Love, "Spot size, adiabaticity and diffraction in tapered fibres," *Electron. Lett.*, vol. 23, pp. 993–994, 1987.
- [32] L. S. Mendes, D. P. Nacaratti, R. E. Samad, and C. C. Motta, "Theoretical analysis of the Efficiency of a  $7 \times 1$  end-pumped power combiner," in *Proc. SBMO/IEEE MTT-S Int. Microw. Optoelectron. Conf.*, 2021, pp. 1–3, doi: [10.1109/IMOC53012.2021.9624827](https://doi.org/10.1109/IMOC53012.2021.9624827).
- [33] D. Stachowiak, "High-power passive fiber components for all-fiber lasers and amplifiers application-Design and fabrication," *Photonics*, vol. 5, no. 4, 2018, Art. no. 38, doi: [10.3390/photonics5040038](https://doi.org/10.3390/photonics5040038).
- [34] W. -P. Huang, "Coupled-mode theory for optical waveguides: An overview," *J. Opt. Soc. Amer. A*, vol. 11, no. 3, pp. 963–983, 1994.
- [35] A. W. Snyder, "Coupled-mode theory for optical fibers," *J. Opt. Soc. Amer.*, vol. 62, no. 11, pp. 1267–1277, 1972.
- [36] F. Gan, "Optical properties of fluoride glasses: A review," *J. Non Cryst. Solids*, vol. 184, pp. 9–20, 1995.
- [37] J. -P. Yehouessi et al., "3 W Mid-IR supercontinuum extended up to  $4.6 \mu\text{m}$  based on an all-PM thulium doped fiber gain-switch laser seeding an InF3 fiber," *Proc. SPIE*, vol. 10902, 2019, Art. no. 1090207.
- [38] A. Annunziato, F. Anelli, P. L. P. D. Teilleul, S. Cozic, S. Poulain, and F. Prudenzano, "Fused optical fiber combiner based on indium fluoride glass: Perspectives for mid-IR applications," *Opt. Exp.*, vol. 30, no. 24, pp. 44160–44174, 2022.
- [39] D. Donlagic, "In-line higher order mode filters based on long highly uniform fiber tapers," *J. Lightw. Technol.*, vol. 24, no. 9, pp. 3532–3539, Sep. 2006.

**Francesco Anelli** (Student Member, IEEE) received the M.Sc. degree in 2021 in electronic engineering (*cum laude*) from Politecnico di Bari, Bari, Italy, where he is currently working toward the Ph.D. degree in electrical and information engineering. His research interests include the design and the characterization of silica optical fiber grating sensors based on novel geometries for curvature, strain, and temperature monitoring, fluoride and chalcogenide fused optical fiber components, such as couplers and combiners for mid-infrared applications.

**Andrea Annunziato** received the M.Sc. degree in electronic engineering (*cum laude*) in 2020 from the Politecnico di Bari, Bari, Italy, where he is currently working toward the Ph.D. degree in aerospace sciences and engineering. His research interests include the design and the characterization of silica optical fiber grating sensors based on planar substrate and flat fiber for curvature, strain, and temperature detection, also in reinforced polymer materials, fluoride, and chalcogenide fused optical fiber components, such as couplers and combiners for all-in-fiber amplifiers and lasers in the mid-infrared spectral range.

**Antonella Maria Loconsole** received the M.Sc. degree in telecommunications engineering (*cum laude*) in 2019 and the Ph.D. degree in electrical and information engineering from Politecnico di Bari, Bari, Italy. She is currently Assistant Professor with Politecnico di Bari. Her research interests include SIW antennas, microwave applicators for medical applications, optical fiber lasers, and amplifiers.

**Vincenza Portosi** received the M.Sc. degree in 2018 in electronic engineering (*cum laude*) from the Politecnico di Bari, Bari, Italy, where she is currently working toward the Ph.D. degree in electrical and information engineering. Her research interests include microwave applicators for medical applications, metamaterials, SIW antennas, and optical fiber sensors.

**Solemn Cozic** received the Ph.D. degree in material science from Rennes 1 University, Rennes, France, in 2016. She is currently a Research and Development Engineer with Le Verre Fluoré. Her research interests include development of novel fluoride glasses, optical fibers, and fluoride glass fiber components for mid infrared, and visible fiber lasers applications.

**Paul Le Pays du Teilleul** is currently with Le Verre Fluoré. His research interests include the fabrication of low-loss fluoride optical fibers and capillaries, and the modeling of optical fiber lasers and amplifiers.

**Sebastien Venck** is currently a Research and Development Engineer with Le Verre Fluoré. His research interests include the modeling and the experiment of Mid-Infrared fiber-based supercontinuum laser source, ICL and QCL pigtailling with fluoride and chalcogenide optical fibers.

**Samuel Poulain** received the Engineering master's degree from ENSTA Paris-Tech, Palaiseau, France, in 1997. After 15 years with Automotive Industry as an Engineer, he became the General Manager of Le Verre Fluoré in 2015. He is involved in various scientific developments, in particular in Mid-IR supercontinuum generation and Mid-IR fiber lasers.

**Francesco Prudeniano** (Member, IEEE) received the Ph.D. degree in electronic engineering from the Politecnico di Bari, Bari, Italy, in 1996. Since 2018, he has been a Full Professor of electromagnetic fields with the Department of Electrical and Information Engineering, Politecnico di Bari. He has coauthored more than 400 publications, 295 of which got published in journals and international conferences, lectures, and invited papers. His research interests include regards the design and characterization of microwave devices, integrated optics, and optical fiber-based devices. He is the Head of Microwave and Optical Engineering Group, Department of Electrical and Information Engineering, Politecnico di Bari. From 2017 to 2018, he was the Chair of SIOF, Italian Society of Optics and Photonics (Italian branch of EOS- European Optical Society). He is involved in several national and international research projects and cooperations.

Open Access funding provided by 'Politecnico di Bari' within the CRUI CARE Agreement